Mendeleev Communications

Mendeleev Commun., 2025, **35**, 234–236

Decomposition of N_2O on different iron-containing catalysts

Anna S. Makova,*[a,b] Alena V. Chesnokova,[b] Alexander L. Kustov,[a,b,c] Alexander V. Leonov,[c] Petr V. Pribytkov,[a,c] Danil S. Plenkin,[c] Marina N. Ter-Akopyan[b] and Leonid M. Kustov[a,b,c]

[a] *N. D. Zelinsky Institute of Organic Chemistry, Russian Academy of Sciences, 119991 Moscow, Russian Federation. E-mail: amakova1997@gmail.com*
[b] *National University of Science and Technology 'MISIS', 119049 Moscow, Russian Federation*
[c] *Department of Chemistry, M. V. Lomonosov Moscow State University, 119991 Moscow, Russian Federation*

DOI: 10.71267/mencom.7530

In this work, Fe-containing catalysts (2.5 wt% Fe) based on different types of materials: zeolites (FER and ZSM-5), silicoaluminophosphates (SAPO-34 and SAPO-5) and titanosilicates (TS-1, AM-4) were studied in the reaction of direct decomposition of N_2O. It was found that the catalytic activity of the obtained catalysts in this reaction was affected both by the content of the Fe active phase and the type and topology of the initial material used for the catalysts preparation.

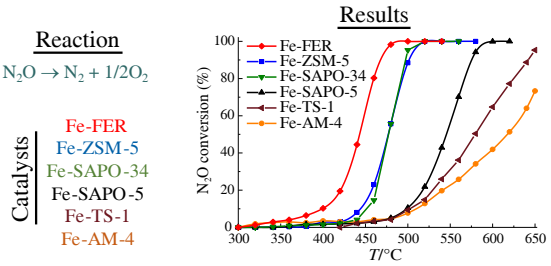

Keywords: N_2O decomposition, iron-containing catalysts, ferrierite, ZSM-5, SAPO-34, SAPO-5, TS-1, AM-4.

Nitrous oxide (N_2O) is a colorless gas that can induce the greenhouse effect and damage the ozone layer.[1] Greenhouse effect caused by N_2O is about 300 times stronger than by CO_2 over a 100-year time scale.[2] In addition, N_2O emission affects human health, primarily due to a decrease in the vitamin B12 (cobalamin) activity.[3] The formation of N_2O occurs in a natural (65%) and anthropogenic (35%) way.[3] The main sources of anthropogenic N_2O include the production of adipic and nitric acids, industrial fertilizers and the combustion of fossil fuels and biomass including car exhausts.[4]

Given the negative impact of N_2O on the environment, an essential task is to reduce emissions of this gas. The simplest and most effective method is direct catalytic decomposition of N_2O. To carry out this reaction, different systems are used, including metal-containing (Fe, Co, Cu and others) zeolites and zeolite-like materials, metal oxides, *etc*.[2,5–9] Nitrous oxide was also used in the oxidation of benzene to phenol on the Fe-ZSM-5 zeolites.[10]

In this work, we compared the catalytic characteristics of Fe-catalysts based on the materials of different types: zeolites (FER, ZSM-5), silicoaluminophosphates (SAPO-34, SAPO-5) and titanosilicates (TS-1, AM-4) in the reaction of N_2O decomposition, taking into account that they demonstrated high activity in this reaction according to published data.[1,11–15] The selected materials were modified with 2.5 wt% Fe, inasmuch as catalysts doped with this metal exhibit high catalytic performance in the N_2O decomposition reaction.[5,16,17] The comparison of the iron-containing catalysts on the certain types of carriers (different zeolites, silicoaluminophosphates, *etc*.) was previously described in many works; however, it is important to note that, prior to our work, there were no studies comparing catalysts with the same iron content on different types of carriers.

Initial samples ZSM-5, SAPO-34, SAPO-5, TS-1, AM-4 were obtained by the hydrothermal (HT) method.[18–22] FER zeolite was synthesized by microwave-hydrothermal (MW) method allowing one to significantly reduce the synthesis time and obtain phase-pure material.[23] Detailed synthesis conditions of samples are presented in Table 1.†

Figure 1 shows the X-ray diffraction patterns of the prepared samples. The phases were identified using the ICDDPDF2 database and the formation of the target phase was confirmed during each synthesis.

The textural properties of the obtained materials are given in Table S1 (see Online Supplementary Materials). All samples except AM-4 exhibit a micro-mesoporous structure.

The chemical composition of the Fe-catalysts is presented in Table S2. The iron content in the obtained catalysts is in the range of 2.13–2.41 wt%.

To identify the iron species, the prepared Fe-containing catalysts were investigated by UV–VIS spectroscopy (see Figure 2). It can be seen that four main bands are presented in the spectra: 260, 318, 392, 512 nm. The bands at 200–300 nm correspond to isolated Fe^{III} ions.[26] The bands in the range 300–400 nm correspond to oligomeric Fe_yO_x species, whereas the bands at 300–350 nm are mostly attributed to binuclear $[HO–Fe–O–Fe–OH]^{2+}$ species, and the bands in the range 350–400 nm are assigned to polynuclear

† The H-forms of FER and ZSM-5 zeolites were obtained *via* ion exchange with a 1 M NH_4NO_3 solution.[21,24] Titanosilicate AM-4 was treated with a 0.5 M HCl solution to obtain the protonated form.[25]

Fe-containing catalysts with the content of the active component of 2.5 wt% were prepared by the incipient wetness method with an iron(III) acetylacetonate solution. The prepared materials were dried at 120 °C and then calcined in air at 600 °C for 7 h.

The prepared samples were investigated by X-ray diffraction (XRD), low-temperature N_2 adsorption/desorption and SEM-EDS methods. The Fe-catalysts were examined by XRD and diffuse reflectance UV–VIS spectroscopy. For a detailed description of methods of the investigation see Online Supplementary Materials (S1).

The N_2O decomposition reaction was carried out in a flow quartz reactor at an atmospheric pressure at temperatures of 300–650 °C, a N_2O flow rate of 5 ml min^{-1} and catalyst loading of 0.1 g.

Table 1 Synthesis conditions of the initial materials.

Samples	Molar composition of the initial gel	*T*/°C	*t*/h	Synthesis method
FER	$6Na_2O : 1SiO_2 : 0.05Al_2O_3 : 1.3EDA : 50H_2O$	190	8	MW
ZSM-5	$20SiO_2 : 1Al_2O_3 : 1TPAOH : 1.5Na_2O : 200H_2O$	180	48	HT
SAPO-34	$3TEA : 0.6SiO_2 : 1Al_2O_3 : 1P_2O_5 : 50H_2O$	200	48	HT
SAPO-5	$2TEA : 0.6SiO_2 : 1Al_2O_3 : 1P_2O_5 : 50H_2O$	200	24	HT
TS-1	$SiO_2 : 0.05TiO_2 : 0.4TPAOH : 1.5C_2H_5OH : 24H_2O$	175	72	HT
AM-4	$5.6Na_2O : 3.1SiO_2 : 1TiO_2 : 130H_2O$	230	96	HT

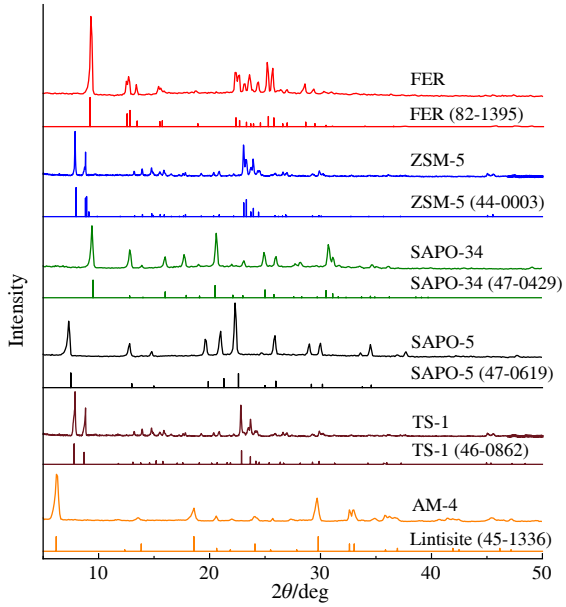

Figure 1 XRD patterns of different synthesized materials and their analogues from ICDDPDF2 database.

FeO_x species.[27,28] The bands above 400 nm correspond to the formation of Fe_2O_3 particles, and the longer the wavelength, the larger particles are formed.[29]

Thus, of all the catalysts studied, Fe-FER and Fe-ZSM-5 had the highest content of Fe^{III} ion species and Fe_yO_x oligomeric species, which represent the active forms of Fe in the N_2O decomposition reaction.[12,30] Also, these zeolite catalysts possessed the largest amount of the inactive phase – large particles of Fe_2O_3.[1,26] The maximum quantity of different Fe species (active and inactive in the N_2O decomposition reaction) has been revealed in the Fe-FER catalyst. The lowest and approximately equal quantity of active Fe species has been demonstrated by the samples Fe-SAPO-34 and Fe-SAPO-5. In the Fe-SAPO-5 sample, the number of FeO_x binuclear species was slightly higher than in the Fe-SAPO-34 sample. The content

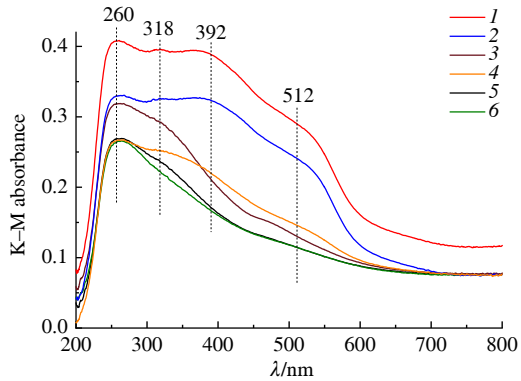

Figure 2 UV–VIS spectra of Fe-catalysts: (*1*) Fe-FER, (*2*) Fe-ZSM-5, (*3*) Fe-TS-1, (*4*) Fe-AM-4, (*5*) Fe-SAPO-5, and (*6*) Fe-SAPO-34.

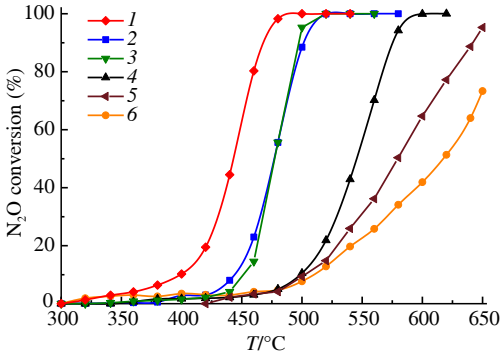

Figure 3 Dependences of the N_2O conversion on the reaction temperature obtained on different Fe-catalysts: (*1*) Fe-FER, (*2*) Fe-ZSM-5, (*3*) Fe-SAPO-34, (*4*) Fe-SAPO-5, (*5*) Fe-TS-1, and (*6*) Fe-AM-4.

of the active phase in Fe-catalysts based on titanosilicates occupies an intermediate position between the catalysts based on zeolites and SAPOs. In this case, the Fe-TS-1 sample contains more Fe^{III} species than Fe-AM-4. Thus, according to the quantity of the active phase, the catalysts can be arranged as follows: Fe-FER > Fe-ZSM-5 > Fe-TS-1 > Fe-AM-4 > Fe-SAPO-5 ≈ Fe-SAPO-34. According to the content of Fe_2O_3 particles and their size, the catalysts can be arranged as: Fe-FER > Fe-ZSM-5 >> Fe-AM-4 > Fe-TS-1 > Fe-SAPO-5 ≈ Fe-SAPO-34. These results correlate with the XRD results of Fe-containing catalysts (see Figure S1 in Online Supplementary Materials).

The data of the catalytic experiments are presented in Figure 3 and Figure S2. The Fe-FER catalyst proved to be the most active in this reaction: a 100% conversion was achieved at 460 °C. Fe-ZSM-5 and Fe-SAPO-34 catalysts demonstrated similar results and showed the highest conversion at 500 °C. The Fe-SAPO-5 catalyst performance was inferior to that of Fe-SAPO-34 and the sample showed a 100% conversion at 580 °C. Titanosilicate-based catalysts performed the worst: at 650 °C, the conversion on the Fe-TS-1 catalyst was about 95% and on the Fe-AM-4 catalyst – about 75%. Thus, according to the activity in the reaction of N_2O decomposition, the catalysts can be arranged as follows: Fe-FER > Fe-ZSM-5 ≈ Fe-SAPO-34 > Fe-SAPO-5 > Fe-TS-1 > Fe-AM-4. Inasmuch as this sequence does not coincide with the order of the active phase content in the catalysts, these results indicate that not only the Fe active phase content, but also the type and topology of the initial material for the preparation of Fe-catalysts affect the catalytic performance in the N_2O decomposition reaction.

In turn, according to the effect of the material type on the catalytic characteristics, the catalysts can be arranged as follows: Fe-zeolites > Fe-SAPO > Fe-titanosilicates. Therefore, it can be concluded that iron-containing zeolites are the best catalysts for this reaction. Both zeolite ZSM-5 and titanosilicate TS-1 have the MFI topology, however catalysts based on them showed different catalytic characteristics in this reaction. This may indicate that Al presence in the framework of the initial material is preferable to Ti, *i.e.*, in this reaction using aluminosilicates is superior to titanosilicates.

In summary, the study of different Fe-containing samples has shown the following regularities. The quantity of Fe^{III} ion species and Fe_yO_x oligomeric species in the catalysts decreased as follows: Fe-FER > Fe-ZSM-5 > Fe-TS-1 > Fe-AM-4 > Fe-SAPO-5 ≈ Fe-SAPO-34. However, according to the activity in the N_2O decomposition reaction, the catalysts have been arranged in a different order: Fe-FER > Fe-ZSM-5 ≈ Fe-SAPO-34 > Fe-SAPO-5 > Fe-TS-1 > Fe-AM-4. This indicates that both the content of the active Fe phase in the catalysts and the type and topology of the initial material affect the catalyst activity. The revealed highest activity of the Fe-FER catalyst in the reaction may be due to the formation of a unique spatial structure of the FER zeolite and Fe ions.

Electron microscopy characterization was performed in the Department of Structural Studies of Zelinsky Institute of Organic Chemistry, Moscow. This work was financially supported by the Ministry of Science and Higher Education of the Russian Federation, project no. 075-15-2023-585.

Online Supplementary Materials

Supplementary data associated with this article can be found in the online version at doi: 10.71267/mencom.7530.

References

1 J. B. Lim, S. H. Cha and S. B. Hong, *Appl. Catal., B*, 2019, **243**, 750; https://doi.org/10.1016/j.apcatb.2018.10.068.
2 S. Li, J. Wang, R. Shang, J. Zhao, Q. Xu, H. Wang and J. Liu, *Mol. Catal.*, 2024, **552**, 113706; https://doi.org/10.1016/j.mcat.2023.113706.
3 Z. Zhuang, B. Guan, J. Chen, C. Zheng, J. Zhou, T. Su, Y. Chen, C. Zhu, X. Hu, S. Zhao, J. Guo, H. Dang, Y. Zhang, Y. Yuan, C. Yi, C. Xu, B. Xu, W. Zeng, Y. Li, K. Shi, Y. He, Z. Wei and Z. Huang, *Chem. Eng. J.*, 2024, **486**, 150374; https://doi.org/10.1016/j.cej.2024.150374.
4 F. Kapteijn, J. Rodriguez-Mirasol and J. A. Moulijn, *Appl. Catal., B*, 1996, **9**, 25; https://doi.org/10.1016/0926-3373(96)90072-7.
5 M. Rutkowska, A. Jankowska, E. Różycka-Dudek, W. Dubiel, A. Kowalczyk, Z. Piwowarska, S. Llopis, U. Díaz and L. Chmielarz, *Catalysts*, 2020, **10**, 1; https://doi.org/10.3390/catal10101139.
6 S. Sklenak, P. C. Andrikopoulos, B. Boekfa, B. Jansang, J. Nováková, L. Benco, T. Bucko, J. Hafner, J. Dědeček and Z. Sobalík, *J. Catal.*, 2010, **272**, 262; https://doi.org/10.1016/j.jcat.2010.04.008.
7 G. Kuz'micheva, V. Chernyshev, G. Kravchenko, L. Pirutko, E. Khramov, L. Bruk, Z. Pastukhova, A. Kustov, L. Kustov and E. Markova, *Dalton Trans.*, 2022, **51**, 3439; https://doi.org/10.1039/D1DT04131B.
8 M. C. Campa, G. Fierro, A. M. Doyle, S. Tuti, C. Catracchia and D. Pietrogiacomi, *Surf. Interfaces*, 2023, **42**, 103502; https://doi.org/10.1016/j.surfin.2023.103502.
9 K. A. Dubkov, N. S. Ovanesyan, A. A. Shteinman, E. V. Starokon and G. I. Panov, *J. Catal.*, 2002, **207**, 341; https://doi.org/10.1006/jcat.2002.3552.
10 G. I. Panov, G. A. Sheveleva, A. S. Kharitonov, V. N. Romannikov and L. A. Vostrikova, *Appl. Catal., A*, 1992, **82**, 31; https://doi.org/10.1016/0926-860X(92)80003-U.
11 L. M. Kustov, S. F. Dunaev and A. L. Kustov, *Molecules*, 2022, **27**, 398; https://doi.org/ 10.3390/molecules27020398.
12 T. Zhang, X. Qin, Y. Peng, C. Wang, H. Chang, J. Chen and J. Li, *Catal. Commun.*, 2019, **128**, 105706; https://doi.org/10.1016/j.catcom.2019.05.013.
13 K. Jíša, J. Nováková, M. Schwarze, A. Vondrová, S. Sklenák and Z. Sobalik, *J. Catal.*, 2009, **262**, 27; https://doi.org/10.1016/j.jcat.2008.11.025.
14 R. A. Schoonheydt, P. Vanelderen and B. F. Sels, *New Future Dev. Catal.: Catal. Rem. Environ. Concerns*, 2013, 399; https://doi.org/10.1016/B978-0-444-53870-3.00013-7.
15 S. L. Suib, J. Přech, E. Szaniawska and J. Čejka, *Chem. Rev.*, 2023, **123**, 877; https://doi.org/10.1021/acs.chemrev.2c00509.
16 T. Ryu and S. B. Hong, *Appl. Catal., B*, 2020, **266**, 118622; https://doi.org/10.1016/j.apcatb.2020.118622.
17 I. Melián-Cabrera, C. Mentruit, J. A. Z. Pieterse, R. W. van den Brink, G. Mul, F. Kapteijn and J. A. Moulijn, *Catal. Commun.*, 2005, **6**, 301; https://doi.org/10.1016/j.catcom.2005.01.004.
18 C. Sun, Y. Wang, A. Zhao, X. Wang, C. Wang, X. Zhang, Z. Wang, J. Zhao and T. Zhao, *Appl. Catal., A*, 2020, **589**, 117314; https://doi.org/10.1016/j.apcata.2019.117314.
19 Y. Yang, L. Xu, Y. Lyu, X. Liu and Z. Yan, *Microporous Mesoporous Mater.*, 2021, **313**, 110857; https://doi.org/10.1016/j.micromeso.2020.110857.
20 Y. Guo, J. Li, L. Zhao, Q. Xu, Z. Song, J. Wang, M. Han, L. Chen, W. Cheng and X. Guo, *Mol. Catal.*, 2024, **560**, 114106; https://doi.org/10.1016/j.mcat.2024.114106.
21 F. Yaripour, Z. Shariatinia, S. Sahebdelfar and A. Irandoukht, *J. Nat. Gas Sci. Eng.*, 2015, **22**, 260; https://doi.org/10.1016/j.jngse.2014.12.001.
22 M. N. Timofeeva, J. V. Kurchenko, G. O. Kalashnikova, V. N. Panchenko, A. I. Nikolaev and A. Gil, *Appl. Catal., A*, 2019, **587**, 117240; https://doi.org/10.1016/j.apcata.2019.117240.
23 A. S. Makova, A. L. Kustov, N. A. Davshan, I. V. Mishin, K. B. Kalmykov, A. A. Shesterkina and L. M. Kustov, *Mendeleev Commun.*, 2023, **33**, 528; https://doi.org/10.1016/j.mencom.2023.06.028.
24 R. C. S. Nascimento, D. P. S. Silva, J. S. R. Solano, R. J. B. Motta, B. J. B. Silva, P. H. L. Quintela, J. G. A. Pacheco and A. O. S. Silva, *Microporous Mesoporous Mater.*, 2024, **366**, 112942; https://doi.org/10.1016/j.micromeso.2023.112942.
25 G. O. Kalashnikova, E. S. Zhitova, E. A. Selivanova, Ya. A. Pakhomovsky, V. N. Yakovenchuk, G. Yu. Ivanyuk, A. G. Kasikov, S. V. Drogobuzhskaya, I. R. Elizarova, Yu. G. Kiselev, A. I. Knyazeva, V. N. Korovin, A. I. Nikolaev and S. V. Krivovichev, *Microporous Mesoporous Mater.*, 2021, **313**, 110787; https://doi.org/10.1016/j.micromeso.2020.110787.
26 B. Zhang, F. Liu, H. He and L. Xue, *Chin. J. Catal.*, 2014, **35**, 1972; https://doi.org/10.1016/S1872-2067(14)60184-4.
27 P. Xie, Y. Luo, Z. Ma, C. Huang, C. Miao, Y. Yue, W. Hua and Z. Gao, *J. Catal.*, 2015, **330**, 311; https://doi.org/10.1016/j.jcat.2015.07.010.
28 J. Wang, H. Xia, X. Ju, Z. Feng, F. Fan and C. Li, *J. Catal.*, 2013, **300**, 251; https://doi.org/10.1016/j.jcat.2013.01.011.
29 M. Iwasaki, K. Yamazaki, K. Banno and H. Shinjoh, *J. Catal.*, 2008, **260**, 205; https://doi.org/10.1016/j.jcat.2008.10.009.
30 T. Zhang, Y. Qiu, G. Liu, J. Chen, Y. Peng, B. Liu and J. Li, *J. Catal.*, 2020, **392**, 322; https://doi.org/10.1016/j.jcat.2020.10.015.

Received: 7th June 2024; Com. 24/7530